Naval Research Laboratory

Washington, DC 20375-5320

NRL/MR/6111--15-9661

The Reduction of NO_x Using Pulsed Electron Beams

HAROLD D. LADOUCEUR

Chemical Dynamics and Diagnostics Branch
Chemistry Division

BRIAN T. FISHER

Navy Technology Center for Safety and Survivability
Chemistry Division

MATTHEW F. WOLFORD

Laser Plasma Branch
Plasma Physics Division

JEFFREY C. OWRUTSKY

Chemical Dynamics and Diagnostics Branch
Chemistry Division

December 30, 2015

REPORT DOCUMENTATION PAGE

Form Approved
OMB No. 0704-0188

1. REPORT DATE *(DD-MM-YYYY)*	**2. REPORT TYPE**	**3. DATES COVERED** *(From - To)*
30-12-2015	Memorandum	January – March 2015

4. TITLE AND SUBTITLE

The Reduction of NO_x Using Pulsed Electron Beams

5a. CONTRACT NUMBER

5b. GRANT NUMBER

5c. PROGRAM ELEMENT NUMBER

6. AUTHOR(S)

Harold D. Ladouceur, Brian T. Fisher, Matthew F. Wolford, and Jeffrey C. Owrutsky

5d. PROJECT NUMBER

5e. TASK NUMBER

5f. WORK UNIT NUMBER

7. PERFORMING ORGANIZATION NAME(S) AND ADDRESS(ES)

Naval Research Laboratory
Code 6111
4555 Overlook Avenue, SW
Washington, DC 20375-5320

8. PERFORMING ORGANIZATION REPORT NUMBER

NRL/MR/6111--15-9661

9. SPONSORING / MONITORING AGENCY NAME(S) AND ADDRESS(ES)

Zerronox Corporation (Zerronox)
1170 E Westleigh Rd.
Lake Forest, IL 60045

10. SPONSOR / MONITOR'S ACRONYM(S)

ZC

11. SPONSOR / MONITOR'S REPORT NUMBER(S)

12. DISTRIBUTION / AVAILABILITY STATEMENT

Approved for public release; distribution is unlimited.

13. SUPPLEMENTARY NOTES

14. ABSTRACT

Experimental and computational work conducted at the Naval Research Laboratory (NRL) to reduce NO_x pollutants in a surrogate flue gas (SFG) is described. The SFG is a simulant for exhaust flue gas from a coal combustion power plant. The technology utilizes a pulsed electron beam to decompose NO and NO_2. The pulsed electron beam is generated using the NRL Electra Facility. The extent of decomposition as a function of electron beam energy is studied. Fourier transform infrared spectroscopy and UV-visible spectroscopy are utilized to identify species and the extent of decomposition after the electron beam bombardment. Spectroscopic results are presented. Thermochemical calculations for possible reactions as a function of temperature are included. This report documents work completed by the NRL Chemistry Division in a collaborative effort with the NRL Plasma Physics Division.

15. SUBJECT TERMS

Pulsed electron beam	FTIR NO_x spectra	Nitrogen dioxide
NO_x reduction	Nitrogen oxide	

16. SECURITY CLASSIFICATION OF:			**17. LIMITATION OF ABSTRACT**	**18. NUMBER OF PAGES**	**19a. NAME OF RESPONSIBLE PERSON**
a. REPORT	**b. ABSTRACT**	**c. THIS PAGE**			Harold D. Ladouceur
Unclassified Unlimited	Unclassified Unlimited	Unclassified Unlimited	Unclassified Unlimited	23	**19b. TELEPHONE NUMBER** *(include area code)* (202) 767-3558

Standard Form 298 (Rev. 8-98)
Prescribed by ANSI Std. Z39.18

CONTENTS

EXECUTIVE SUMMARY

This report documents work completed by the Naval Research Laboratory (NRL) Chemistry Division in a collaborative effort with the Plasma Physics Division. Experimental and computational work done at the NRL to reduce NOx pollutants in a surrogate flue gas (SFG) is described. The SFG simulates exhaust flue gas from a coal combustion power plant. The technology utilizes a pulsed electron beam to decompose NO and NO_2. The pulsed electron beam is generated using the NRL Electra Facility. The extent of decomposition as a function of electron beam energy is studied. Fourier-transform infrared spectroscopy (FTIR) and UV-visible spectroscopy are utilized to identify species and the extent of decomposition after the electron beam bombardment. Spectroscopic results are presented. Thermochemical calculations for possible reactions as a function of temperature are included. Water vapor in the SFG reduces the NOx reduction efficiency of the pulsed electron beam.

THE REDUCTION OF NO_x USING PULSED ELECTRON BEAMS

NO_X AND OXIDES OF NITROGEN

The primary motivation for this research was to use a pulsed electron beam to reduce NO_X emissions. In atmospheric chemistry, the term NO_x refers to the total concentration of nitric oxide (NO) and nitrogen dioxide (NO_2) in air. These gases are produced from endothermic reactions between nitrogen and oxygen during high-temperature combustion in air-breathing engines and coal power plants. The gases are also produced in nature during thunderstorms by lightning discharges. In the presence of sunlight and volatile organic compounds, NO_x reacts to form smog, which damages lung tissue. Both nitric oxide and nitrogen dioxide react with atmospheric moisture to produce nitrous acid (HNO_2) and nitric acid (HNO_3), both components of acid rain

$$4NO + 3O_2 + 2H_2O \rightarrow 4HNO_3$$

$$2NO_2 + H_2O \rightarrow HNO_2 + HNO_3$$

$$3HNO_2 \rightarrow HNO_3 + 2NO + H_2O$$

There are several other known oxides of nitrogen [1]. All of the oxides of nitrogen are thermodynamically unstable (Figure 1 Gibbs free energy $\Delta G° > 0$) with regard to elemental oxygen (O_2) and nitrogen (N_2). Since all of these gases are thermodynamically unstable, any process, e.g. a pulsed electron beam, which can break the bonds between the constituent atoms, offers the possibility of producing lower energy state, nontoxic products. The combustion of coal produces carbon dioxide (CO_2) and possibly sulfur dioxide (SO_2). The Gibbs free energy of formation for CO_2 is -394 kJ/mole and for SO_2 the free energy of formation is -300 kJ/mole. These large negative values of free energy indicate that both of these gases are extremely stable when compared to the oxides of nitrogen.

In developing possible kinetic mechanisms for NO_x reduction, one needs to be aware of properties of these various nitrogen oxides in order to exclude unlikely reactants or products. Nitrous oxide (N_2O) is a colorless and rather unreactive gas at room temperature, but it decomposes at 500°C to oxygen and nitrogen. It is nontoxic. Nitrous oxide is used as an anesthetic (laughing gas) and propellant in whipped cream cans. Nitric oxide (NO) is a colorless gas which reacts almost instantly with oxygen to form the brown gas NO_2. Nitrogen dioxide is toxic. Dinitrogen trioxide (N_2O_3) exists as a deep blue solid (-21°C), but is extensively dissociated in the gas phase [2]

$$N_2O_3 = NO + NO_2$$

Dinitrogen pentoxide (N_2O_5) is a colorless, unstable gas which reacts rapidly with water to form nitric acid. Dinitrogen tetroxide (N_2O_4) is extensively dissociated to NO_2 as a gas.

$$N_2O_4 = 2NO_2$$

The important nitrogen-oxide species that should be included in a gas-phase kinetic model are: N_2O, NO, NO_2 and N_2O_4. In the presence of <u>liquid</u> water, nitrous and nitric acid should be included based upon the thermodynamic calculations shown below. Dinitrogen trioxide (N_2O_3) and dinitrogen pentoxide (N_2O_5) can most likely be excluded.

Manuscript approved December 1, 2015

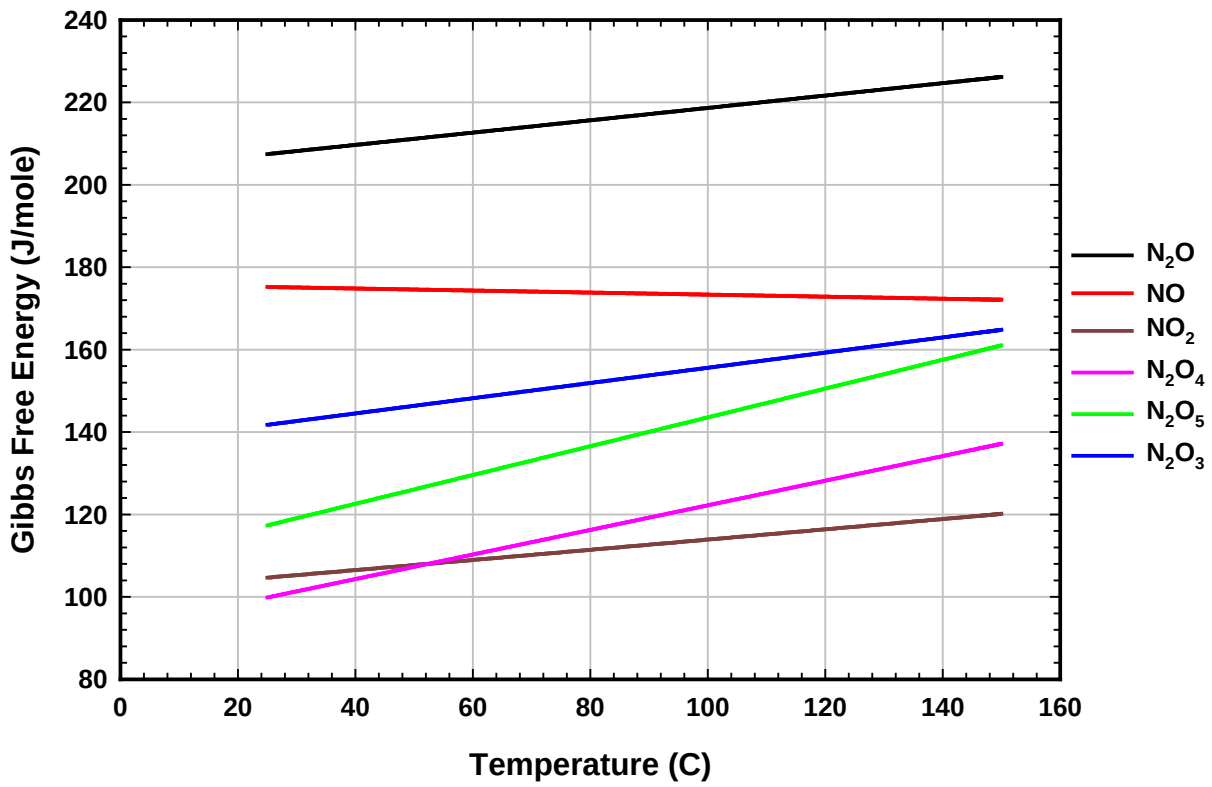

Figure 1. Gibbs free energy of formation of various nitrogen oxides

EQUILIBRIUM CALCULATIONS

Thermodynamic calculations are useful in identifying the possible products in a chemical reaction under the given conditions of temperature, pressure and initial reactant concentrations. A measure of the extent of a reaction going to completion is given by the equilibrium constant K_{eq}. If the equilibrium constant is very small, the chemical reaction is not very likely to occur as written. As a simple example, consider the reaction of nitric oxide (NO) with oxygen (O_2) to form nitrogen dioxide (NO_2). The base-ten logarithm of the equilibrium constant for this reaction is plotted in Figure 2 (solid blue line) as a function of temperature in degrees Centigrade. The temperature range on the x-axis is chosen to correspond to coal power plant operating conditions. The flue gas temperature near the power plant boiler is roughly 150°C and the calculated equilibrium constant is 2.6×10^6. At the exhaust stack, the temperature is 66-71°C and the equilibrium constant is 9.8×10^9. These large values of the equilibrium constant indicate that the formation of nitrogen dioxide is highly favored thermodynamically over the range of the plant's operating conditions. The reaction is also exothermic (ΔH= -114 kJ/mole) which is why the equilibrium constant for the formation of NO_2 is larger at the lower exhaust stack temperature. The equilibrium constant for the reverse reaction ($2NO_2 = 2NO+O_2$) as a function of temperature is also plotted in Figure 2 as a solid red line. Note that the plot lies below zero. Any reaction whose $\log K_{eq}$ is below zero ($K_{eq} < 1$) is unlikely to occur. Thus, the dimerization reaction of nitrogen dioxide (NO_2) to form dinitrogen tetroxide (N_2O_4) (solid

green line) is not favored over the specified temperature range until the flue gas temperature drops below 50°C.

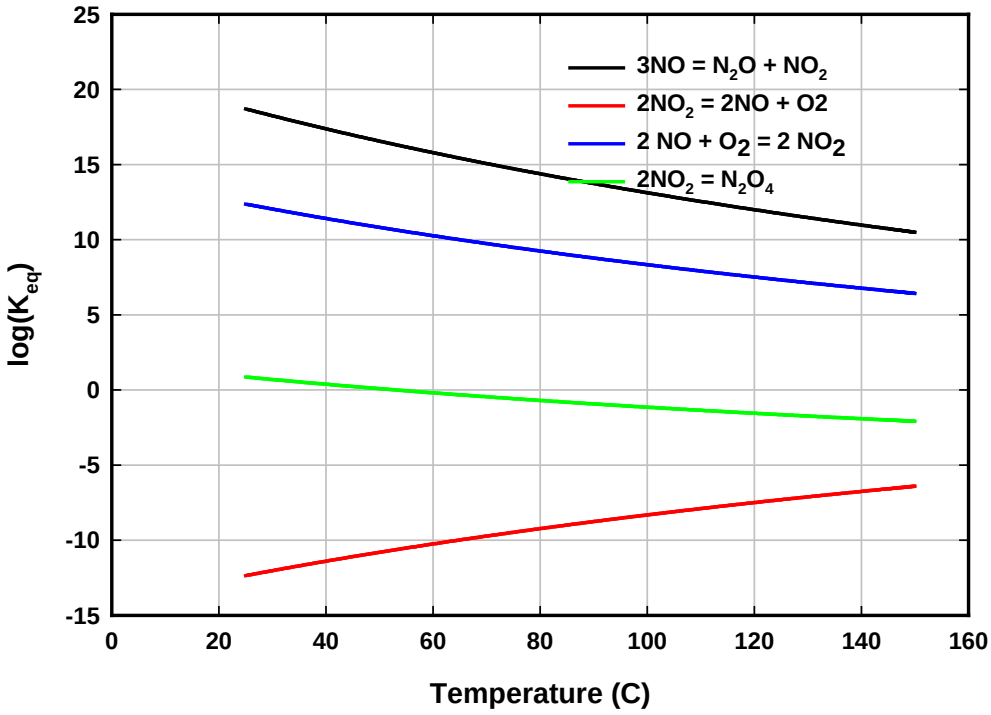

Figure 2. Equilibrium constants as a function of temperature for various reactions of nitrogen oxides

Equilibrium calculations are also useful in predicting if a particular chemical species can exist under given conditions of temperature and pressure. However, the calculations tell nothing about the rates at which the reactions proceed. At equilibrium, the forward and reverse reaction rates are equal. Given a forward rate constant, the equilibrium constant can be used to calculate the reverse rate constant by the law of mass action. This is useful in developing and implementing a kinetic mechanism since reverse reaction rates are often not measured.

Figure 3 shows the calculated equilibrium constants for the reactions of various nitrogen oxides with liquid water, H_2O (l), and water vapor to form both gaseous HNO_3 and HNO_2 and liquid acids (a). The liquid phase reaction (green line) for the formation of nitrous and nitric acid is favored over the gas phase reactions for temperatures below 100°C. In the coal power plant, the SO_2 scrubber, which uses liquid water droplets, operates over temperature ranges from 60-80°C. Over this range the equilibrium constant for the formation of liquid acids varies from 100 to 18.

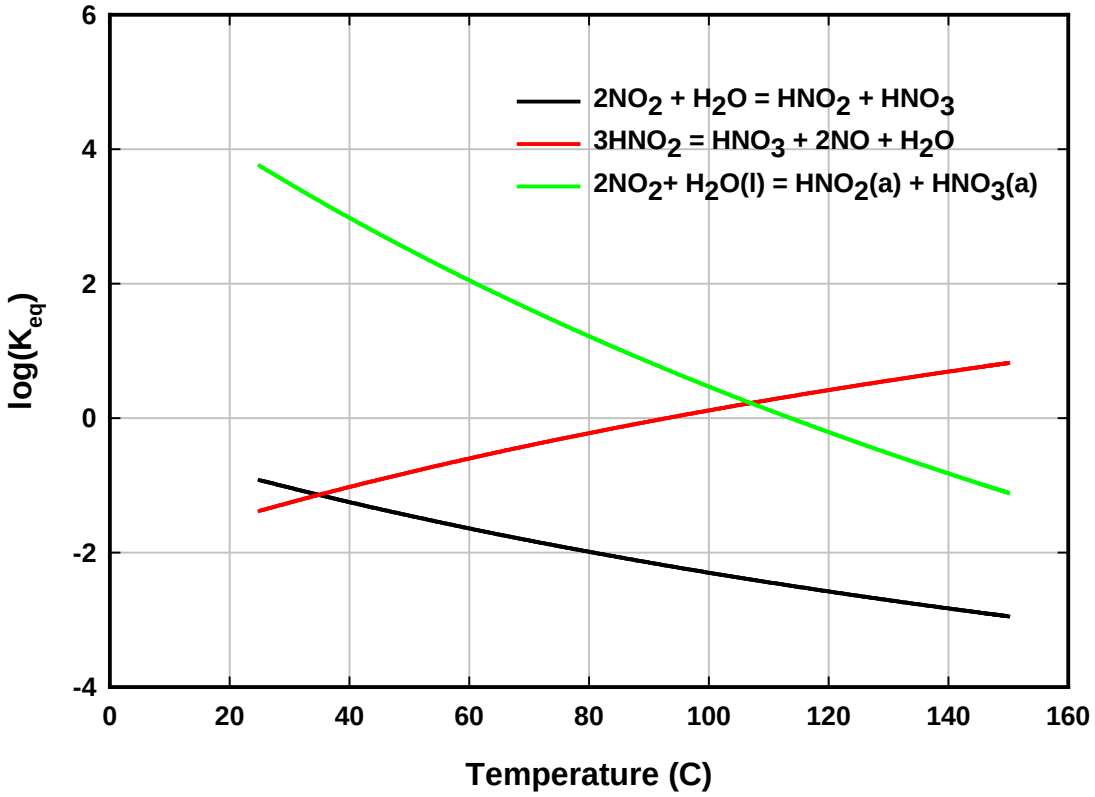

Figure 3. Equilibrium constants for NO_x reactions with H_2O. The (l) and (a) denote liquid and aqueous states

Combustion of coal containing sulfur produces sulfur dioxide (SO_2) which is removed by water scrubbers. The scrubbers operate in a temperature range of 60-80°C. Sulfur dioxide (SO_2) reacts with water to form sulfurous acid (H_2SO_3). The equilibrium constant for this reaction is on the order of 1.33 at 65°C and increases to 43 at 25°C. Near the boiler, the flue gas temperature of 150°C lowers the equilibrium constant to 5.7×10^{-3}. The removal of SO_2 can be enhanced by the use of an aqueous base solution which shifts the equilibrium.

GENERATION OF PULSED ELECTRON BEAM

The experiments reported below were performed in the Naval Research Laboratory's Electra facility [3-4]. The Electra facility was designed to optimize the performance of a 248 nm repetitively pulsed (5 Hz) KrF laser system for power production via laser fusion energy [5]. The Electra main amplifier in KrF laser mode contains two identical pulse power systems which produce counter-propagating, 500 keV, flat-top 140-ns full width at half maximum, repetitively pulsed electron beams into a 30 cm x 30 cm x 100 cm electron beam pumped volume with a laser gas cell. Subsequently, Electra has been reconfigured to examine the mitigation of NO_x utilizing pulsed electron beams [6]. This configuration is depicted in Figures 4a and 4b.

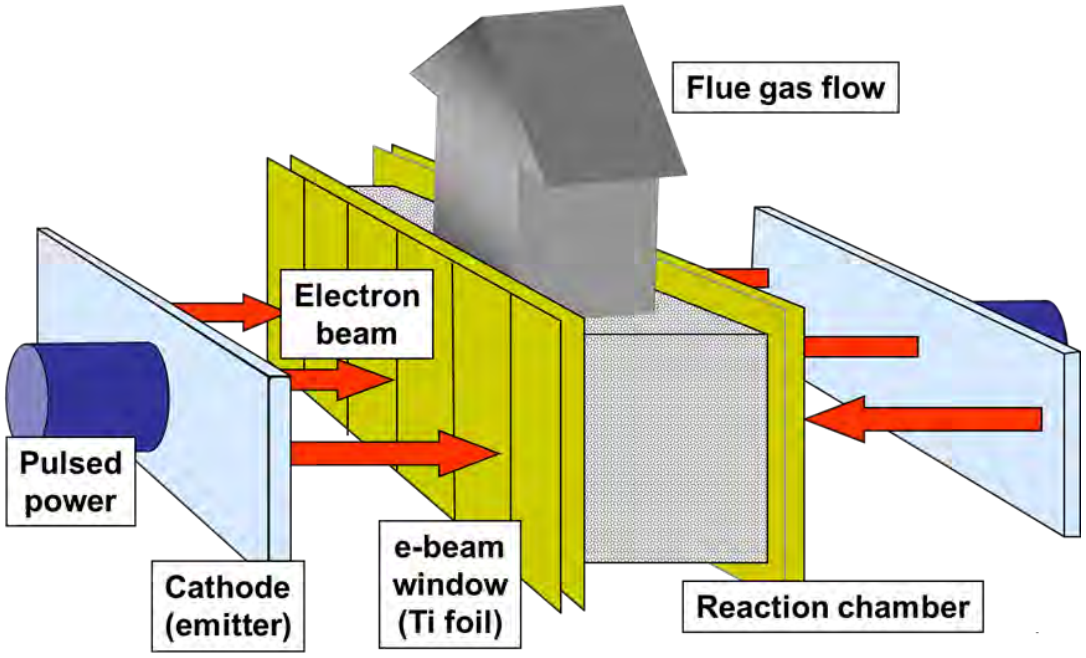

Figure 4a. Experimental configuration

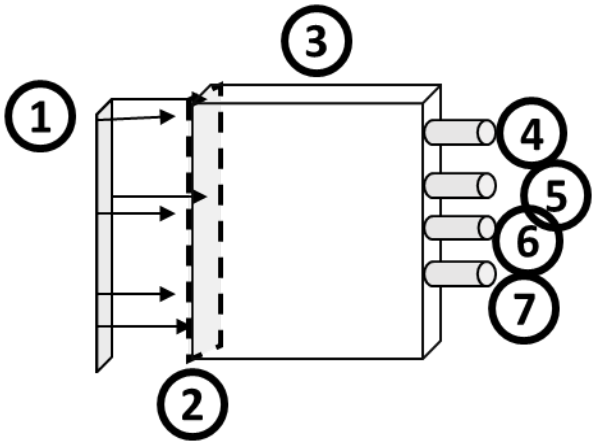

Figure 4b. Components of NO_x removal Electra experiments. 1) Cathode, 2) Titanium foil and support structure, 3) Reaction chamber (Aluminum), 4) Pressure transducer, 5) Gas inlet, 6) Sample line, 7) Gas exhaust

In the experiments depicted here a single electron beam shot was used as opposed to multiple electron beam shots as reported previously [6]. The electron beam aperture was the same at 11.7 cm x 29.6 cm as in the previous NO_x removal experiments. In order to increase the deposited energy into the gas on a single shot,

the velvet cathode was decreased in area to 30.2 cm x 15.5 cm from 28 cm x 98 cm. The increased energy deposition in the 51 μm thick titanium foil from the electron beam traveling through the material as well as the increased pressure rise from the electron beam shot required a center vertical rib 29.6 cm x 1cm x1 cm. The voltage for the experimental data in Table 1 ranged from 500 keV – 750 keV depending on the Electra charging voltage. Additional attenuation of the energy deposited in the gas was attained by placing screens directly in front of the foil within the diode box. The additional attenuation for 2015-03-17 was a 25% optical transparent perforated plate. For the shots 2015-03-26, 2015-03-31, and 2015-04-01 two stainless steel screens with an optical transparency of 64% overlapped with each other were used. This configuration of Electra allowed the ability to scan energy deposition without making any changes to the gaseous deposition volume.

Table 1. Experimental Conditions

Date	E-beam energy deposition	Gas mixture	Gas temp.	Gas press.[1]
2015-03-10	840 J	1000 ppm NO_x[2] Balance N_2	Room	129 kPa
2015-03-17	226 J	SFG[3] (dry)	79°C	125 kPa
2015-03-26	322 J	SFG[3] (humid)	Room	150 kPa
2015-03-31	300 J	SFG[3] (humid)	79°C	132 kPa
2015-04-01	419 J	SFG[3] (humid)	79°C	143 kPa

[1] Pressure in gas mixture before beam shot (pressure is always lower after beam shot)
[2] Nominal value; measured concentrations of NO and NO_2 are shown below in results
[3] SFG (surrogate flue gas) = 11.5% CO_2, 6.465% O_2, 99.5 ppm NO_x, 55.5 ppm SO_2, balance N_2

The deposition volume for these experiments was an aluminum box attached to a support structure which resembles a hibachi, where the vertical rib represents a single cross member, and through which the electron beam passes. A Teflon insert is placed between the aluminum box and the hibachi to allow heating experiments. The total contained volume for these experiments was 14.0 liters including all ports. Shut-off valves were placed as close as possible to the aluminum box to avoid unpumped electron beam regions as much as possible. The aluminum box and insert are slightly oversized to the electron beam aperture to minimize electrons being directly deposited into the box. The electron beam pumped volume is composed of the electron aperture with a depth to the back of the aluminum box of 33.6 cm. Therefore the electron beam pumped volume is 11.6 liters. The percentage volume of electron beam pumped region (treated volume) to total volume is 83%. This is an improvement over previous experiments in which treatment for a single shot was only 43% of the total volume [6].

The amount of energy deposited in the reaction chamber was measured using a pressure transducer to measure the pressure rise in the gas from the deposited electron beam energy. The procedure and evaluation of using the pressure transducer with a 3% radiation correction factor for radiation losses is reported elsewhere [7].

SPECTROSCOPIC MEASURMENTS

The objectives of these experiments were to use spectrometric measurements to survey the species present before and after electron-beam treatment of various gas mixtures, to evaluate detection limits and sensitivities for the instruments, and to determine the effect of water vapor on the effectiveness of the electron beam in reducing NO_X levels.

Electron-beam treatments, or "beam shots," were conducted for several different conditions in this study, as listed in Table 1. A single beam shot was conducted on each of the days listed. For each experiment, the chamber was filled with the appropriate gas mixture to the chosen pressure. In some experiments, this chamber was then heated to a specified temperature, typically 79.4°C (175°F); in other experiments, the gas mixture in the chamber remained at room temperature. The gas mixture was typically held in the chamber for 1-2 hours before electron-beam treatment.

Both before and after each beam shot, gas samples were extracted into a 10 cm pathlength stainless-steel gas cell (100 ml) outfitted with CaF_2 windows for broad UV/visible/IR transmission. The nominal pressure within the cell was one atm. Pre-beam gas samples were extracted approximately 30 to 45 minutes before the beam shot; post-beam gas samples were extracted within 10 to 15 minutes after the beam shot. Each time a sample was extracted, measurements were taken using a Nicolet FTIR (Fourier transform infrared) spectrometer and a Perkin-Elmer UV-Visible spectrometer. Because it was necessary to transport the gas cell to a separate building from the "Electra" facility, a process which typically took 10 minutes, all samples were assumed to be at room temperature at the time of each measurement. Measurement parameters used in this study for each spectrometer are listed in Table 2. The spectral resolutions were chosen to be similar to pressure broadened linewidths under the conditions of one atmosphere of pressure to avoid reducing the line intensities and degrading the sensitivities.

Table 2. Spectroscopic measurement parameters used in this study

	Model	Measurement parameters
FTIR	Nicolet 6700	Resolution = 0.125 cm^{-1} Range = (650 – 4000) cm^{-1} # scans = 16
UV-Vis	Perkin-Elmer Lambda 1050	Resolution = 1 nm Slit width = 1 nm Range = (180 – 500) nm # scans = 1

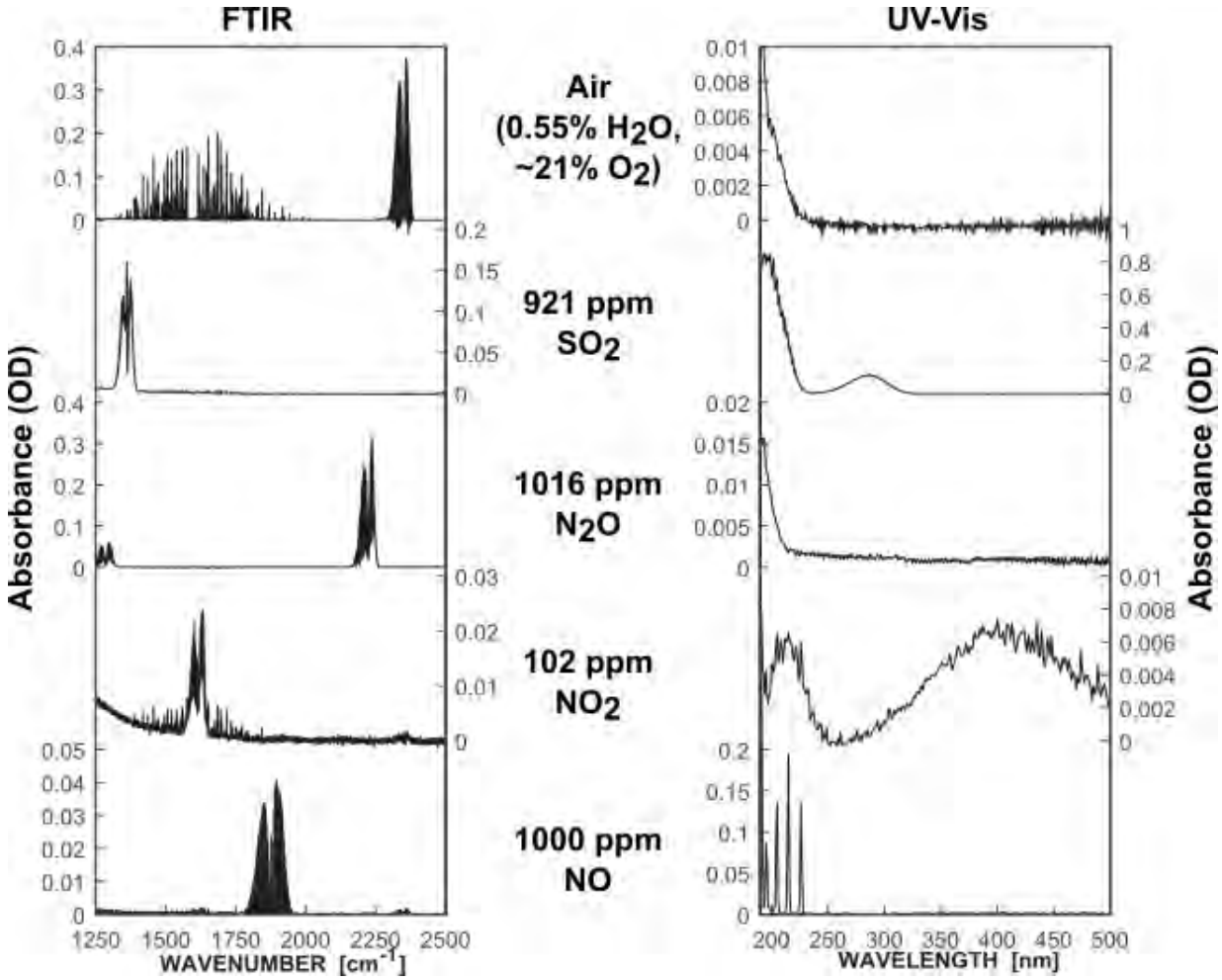

Figure 5. Reference absorbance spectra taken in a 10 cm pathlength cell. For each case (except air), balance of sample to one atmosphere was nitrogen

Species of primary interest in this study included NO, NO_2, N_2O, and H_2O (vapor). Spectra were recorded for reference gas mixtures in order to obtain quantitative data for these and other species (e.g., SO_2) from the electron-beam experiments. For each species, a reference spectrum was recorded for only one concentration, and that concentration was considerably higher than levels in the electron-beam experiments (e.g., 1000 ppm NO in reference experiment vs. 100 ppm NO in the electron-beam experiment at a total pressure of one atmosphere). The spectral resolution used was chosen to be similar to pressurized broadened linewidths. Otherwise, the sensitivity would be lower. Thus, quantities reported here are approximate; higher-accuracy measurements will require detailed calibrations with spectra recorded at multiple concentrations for each species. Reference FTIR and UV-Vis absorbance spectra (OD = optical density) are shown in Figure 5, where the balance gas for each species of interest (except air) was nitrogen.

SPECTROSCOPIC RESULTS

As Table 1 shows, a variety of conditions were used to test the NO_X-reduction potential of the e-beam in a systematic manner, starting from a simple mixture of 1000 ppm NO_X in N_2, followed by dry SFG (surrogate flue gas), then humid SFG at room temperature, then humid SFG at elevated temperature, and finally humid SFG at elevated temperature with higher e-beam energy. Overview FTIR and UV-Vis spectra are shown in Figure 6, with relevant species features labeled, for the first 4 beam shots (through 2015-03-31).

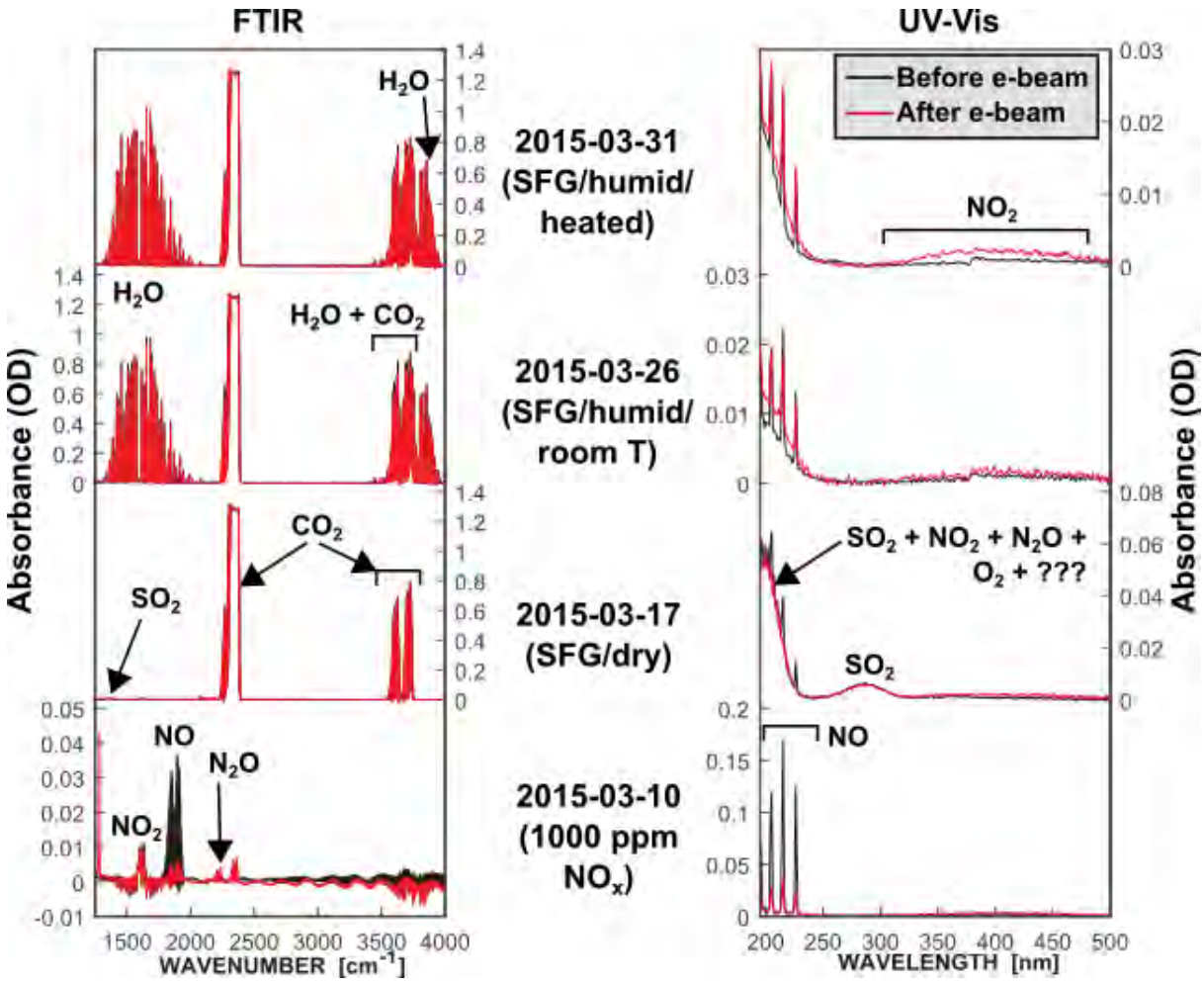

Figure 6. Absorbance spectra, showing the entire spectral ranges of the measurements

In the FTIR spectra, the absorption features of NO, NO_2, and N_2O are clearly visible in the 2015-03-10 data because there was no CO_2 or H_2O to contend with in the mixture. On the other days, however, there were high levels of these latter species in the SFG that led to large absorbances which swamped the signals of the other species. In some of the UV-Vis spectra, there was broad absorption below 250 nm that is due to additive absorbance from SO_2, NO_2, N_2O, and O_2, which are illustrated individually in the reference spectra of Figure 5. The contribution of SO_2 was missing on 2015-03-26 and 2015-03-31, as evidenced by the lack of absorption between 250 nm and 300 nm. Thus, we conclude that SO_2 is either reacting directly with H_2O

or reacting with something else facilitated by H_2O, since SO_2 absorption was present when the SFG was dry but missing when the SFG was humid.

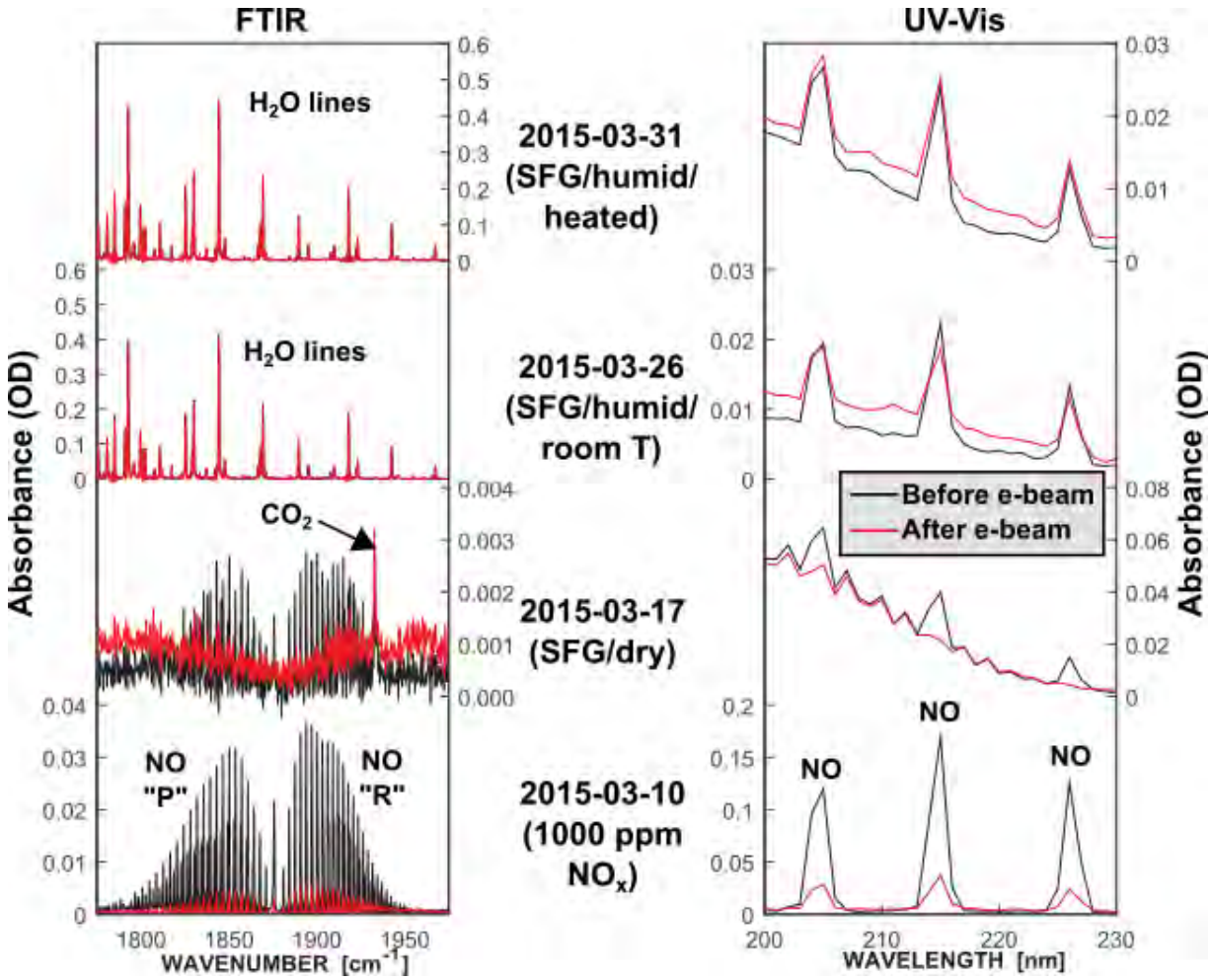

Figure 7. Absorbance spectra, showing regions of interest for NO absorption

Further details can be seen by zooming in on various spectral regions. Shown in Figure 7 are the same spectra, but focusing on regions of interest for NO absorption. In the FTIR spectra, both the P and R branches of the NO absorption band were clearly visible for the 2015-03-10 data both before and after the beam shot, while they were only clearly visible before the beam shot for the 2015-03-17 data. For the humid SFG mixtures, however, water lines created strong interference in this spectral region. Of note is a CO_2 overtone absorption feature at approximately 1933 cm^{-1}, which is only visible on 2015-03-17 due to the weakness of the nearby NO absorbance. The UV-Vis spectra show clear NO absorption for all of the data, though the spectrum after the beam shot on 2015-03-17 shows very modest, if any, NO absorption above the broad absorption baseline. A significant conclusion supported by the UV-Vis spectra in Figure 7 is that the e-beam is highly effective at reducing NO_x when no water vapor is present, but not nearly as effective when it is present.

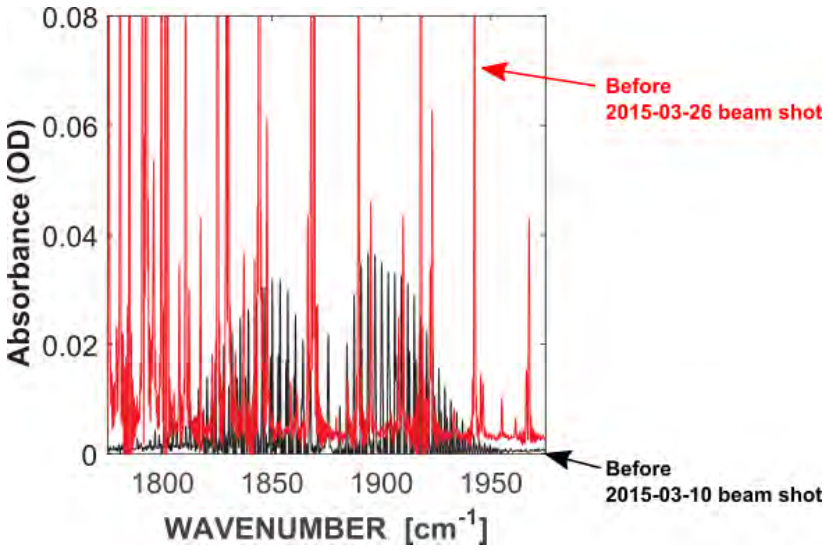

Figure 8. FTIR spectra illustrating water vapor interference with respect to NO absorption

We also conclude that it is better to use UV-Vis measurements than FTIR to quantify NO, since it is free of water interference. Figure 8 shows two FTIR spectra, one with water vapor present and one without, to illustrate the difficulty in getting both NO absorbance signal and baseline when water vapor is present.

Shown in Figure 9 are all of the measured spectra, but focusing on regions of interest for NO_2 absorption. Both the P and R branches of the absorption band are visible in the FTIR spectra for which no water vapor was present, both before and after the beam shots. The UV-Vis spectra show weak but clear, broad NO_2 absorption from approximately 300 nm to 500 nm. It was necessary, however, to avoid using the lower portion of that region for NO_2 quantification due to potential SO_2 interference. For the humid SFG mixtures, water lines created strong interference in the FTIR spectra, as shown in Figure 9 and in the closer-up view in Figure 10. Although it may be possible to isolate an area of the P branch of NO_2 absorption that is interference-free, there is the additional issue of detection limit since NO_2 levels were so low. Thus, we conclude that it is better to use UV-Vis than FTIR to quantify NO_2. From the UV-Vis spectra, it is clear that the electron beam actually caused NO_2 levels to increase, and more so when the gas was heated.

Shown in Figure 11 are all of the measured FTIR spectra, but focusing on a region of interest for N_2O absorption. UV-vis spectra are not shown in this case because there is minimal absorbance for N_2O in the UV-visible region; N_2O absorption merely adds to the broad absorbance below ~225 nm, and its contribution is extremely weak (see Figure 5). Considering the FTIR spectra in Figure 11, there are two issues with N_2O quantification. The first issue is interference from CO and CO_2 absorption. This can be overcome, however, since there is enough spacing between the CO lines to extract N_2O absorption information and also because the CO_2 absorption band is not strong enough to interfere near 2230 cm^{-1}. The second and more difficult issue is sensitivity, since N_2O concentrations were so low. For all of the measurements using SFG (i.e., excluding the 2015-03-10 measurement for which initial gas mixture was

1000 ppm NO_X) the calculated N_2O volume fractions after the beam shots were at the single-digit-ppm level. We do not consider these values trustworthy since the N_2O signals were buried in the noise.

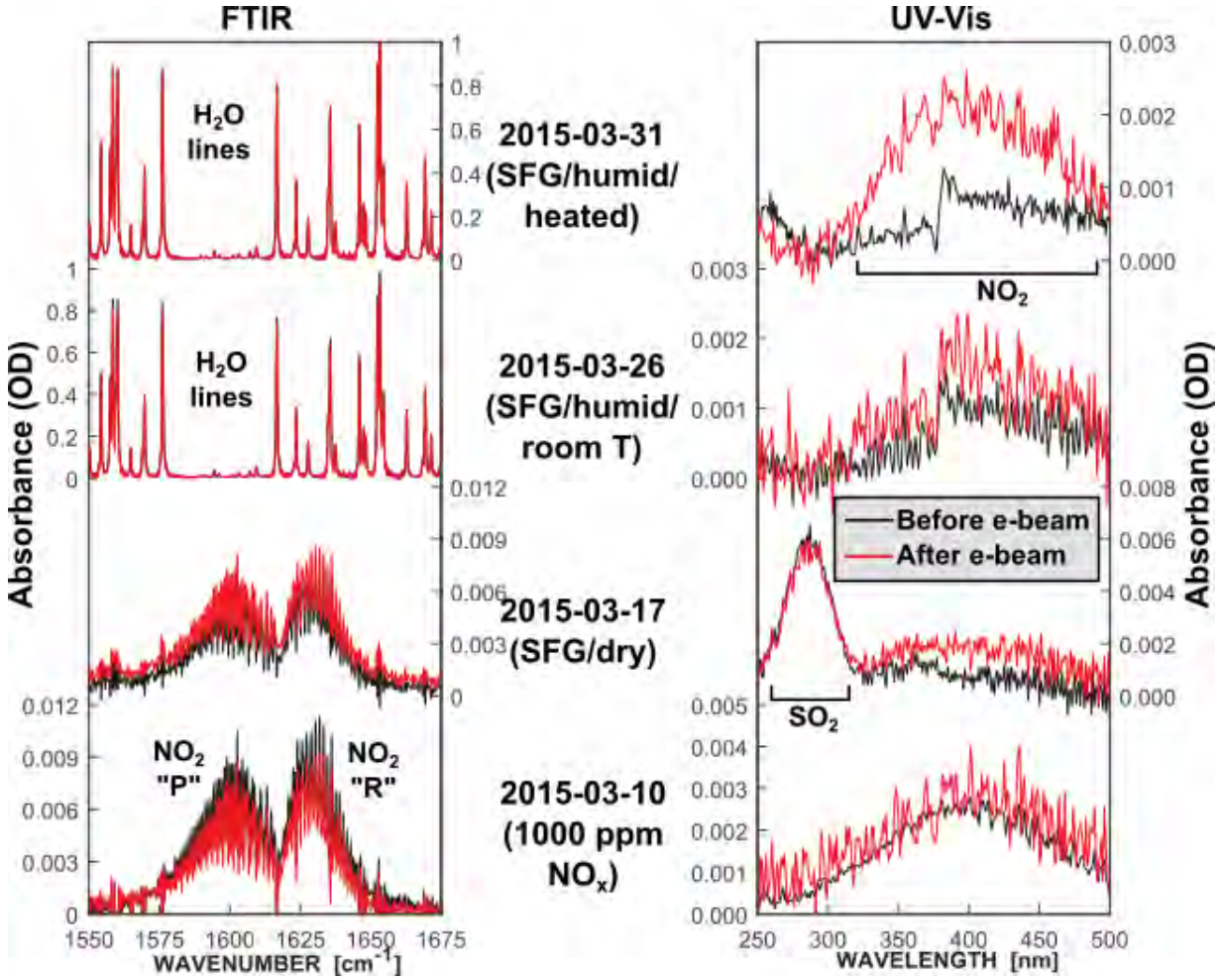

Figure 9. Absorbance spectra, showing regions of interest for NO_2 absorption

Shown in Figure 12 are all of the measured FTIR spectra, but focusing on a region of interest for SO_2 absorption. UV-vis spectra are not shown in this case because Figure 6 (right column) already illustrates the useful information about SO_2 in the UV-visible absorption. The UV-vis spectra in Figure 6 show that there was no evidence of SO_2 on 2015-03-10, as expected since the gas mixture was 1000 ppm NO_x in N_2. There was clear evidence of SO_2 on 2015-03-17, where the gas was dry SFG, but it is noted that the e-beam appeared to have no effect on SO_2 since it seems to have the same absorbance both before and after the beam shot. This observation is consistent with the thermodynamic stability of SO_2 (-300 kJ/mole). Interestingly, on the other days where the gas was humid SFG, there was no evidence of SO_2 either before or after the beam shot. This suggests that SO_2 reacts with water vapor in this system, though it is not yet clear what happens to the product(s) of this reaction. The FTIR spectra in Figure 12 reinforce all of these observations, namely the lack of any SO_2 presence on any day except 2015-03-17 (dry SFG) and minimal

to no change in SO_2 absorbance due to the beam shot on 2015-03-17. We note also that there are several water absorption lines that overlap SO_2 infrared absorption. Thus, even if SO_2 were present in the FTIR spectra from the humid SFG mixtures it would be nearly impossible to quantify the concentrations.

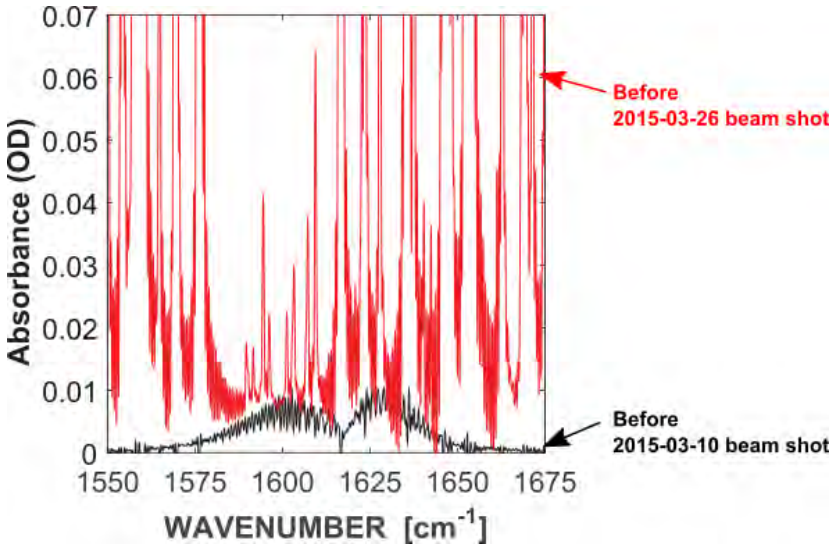

Figure 10. FTIR spectra illustrating water vapor interference with respect to NO_2 absorption

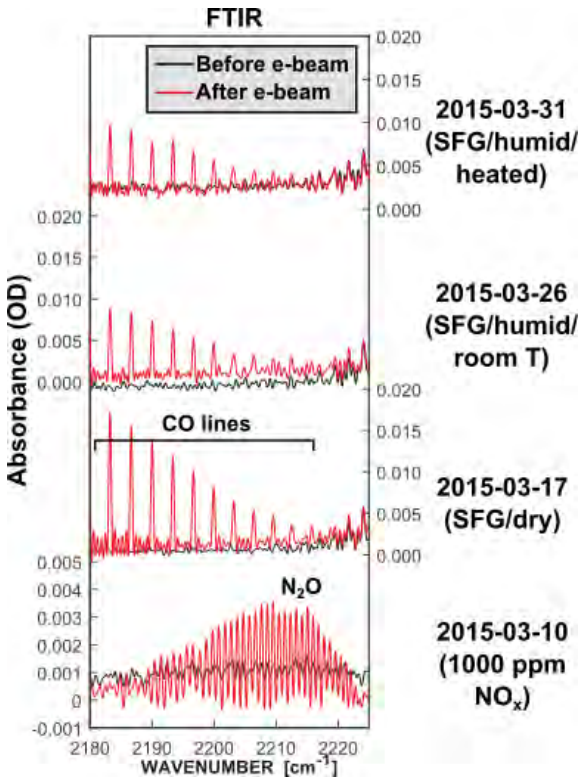

Figure 11. Absorbance spectra showing regions of interest for N_2O absorption

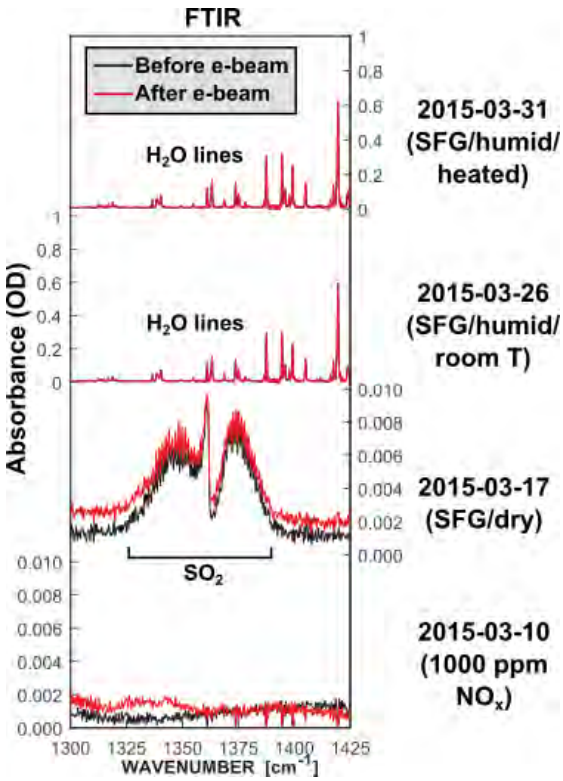

Figure 12. Absorbance spectra showing regions of interest for SO_2 absorption

By comparing the recorded FTIR and UV-Vis spectra with the reference spectra shown in Figure 5, we were able to evaluate quantitative concentrations for some of the species of interest. While these measurements may be considered quantitative, they should be considered more as estimates since they are based on single-point calibrations (i.e., reference spectra were only recorded for a single concentration). For future measurements, we will perform careful, multi-point calibrations for appropriate concentration levels of each species and thereby make the determined concentrations more robust. Species volume fractions before and after electron-beam treatment are shown in Tables 3 and 4 and plotted in Figures 13-15. As discussed in detail above, much of the FTIR-based data were deemed unreliable, mostly due to interference from water vapor absorption lines. For cases where FTIR and UV-Vis data were both considered reliable, there is generally good qualitative, and to some extent quantitative, agreement between the two measurements. On 03-10-2015, for example, measurements of NO, NO_2, and total NO_X are very similar between the FTIR and the UV-Vis data.

The primary motivation for this research was to use a pulsed electron beam to reduce NO_X emissions; thus, it is important to examine the NO_X measurements. An important first observation is that the electron beam was very effective at reducing NO when the gas mixture was simply 1000 ppm NO_X in N_2 (on 03-10-2015), with a final volume fraction of only ~15–20 % of the original value. The same nominal effect was also observed when the gas mixture was dry SFG (on 03-17-2015). When the gas mixture was humid SFG, however, results changed considerably. For humid SFG at room temperature, final NO volume fraction was ~67% of initial. For humid SFG heated to 79°C, final NO volume fraction was ~93% of initial. For humid SFG heated to 79°C with higher e-beam energy deposition, final NO volume fraction was ~114% of initial, meaning that the electron beam in this case actually helped to *create* additional NO. Regardless of conditions, NO_2 generally did not change much but tended to increase slightly after e-beam treatment.

Table 3. Species volume fractions before and after electron-beam treatments based on FTIR measurements (unreliable data are shown in gray boxes)

Volume fractions (ppm)	03-10	03-17	03-26	03-31	04-01
NO [ppm]	891 → 131	57 → 8	397* → 378*	417* → 430*	359* → 371*
NO_2 [ppm]	53 → 39	31 → 32	28* → 30*	18* → 29*	28* → 42*
Tot. NO_X [ppm]	944 → 170	88 → 40	425* → 408*	435* → 459*	387* → 413*
N_2O [ppm]	6** → 13**	3** → 6**	4** → 5**	2** → 4**	3** → 10**
SO_2 [ppm]	0** → 1**	45 → 40	14* → 12*	14* → 13*	11* → 13*
H_2O [%]	0.0** → 0.0**	0.0** → 0.0**	2.5 → 2.4	2.6 → 2.6	2.3 → 2.4

* Data unreliable due to interference from water vapor absorption lines

** Data likely below detection limit

Table 4. Species volume fractions before and after electron-beam treatments based on UV-Vis measurements (unreliable data are shown in gray boxes)

Volume fractions (ppm)	03-10	03-17	03-26	03-31	04-01
NO [ppm]	918 → 176	112 → 20	87 → 58	84 → 78	81 → 92
NO_2 [ppm]	39 → 46	12 → 30	15 → 24	13 → 33	0 → 51
Tot. NO_X [ppm]	957 → 222	124 → 50	102 → 82	97 → 111	81 → 143
SO_2 [ppm]	$10^{*} \rightarrow 24^{*}$	52 → 52	$8^{*} \rightarrow 11^{*}$	$15^{*} \rightarrow 11^{*}$	$7^{*} \rightarrow 92^{**}$

* Data likely below detection limit

** Data unreliable due to unidentified issue (possibly interference from unknown species)

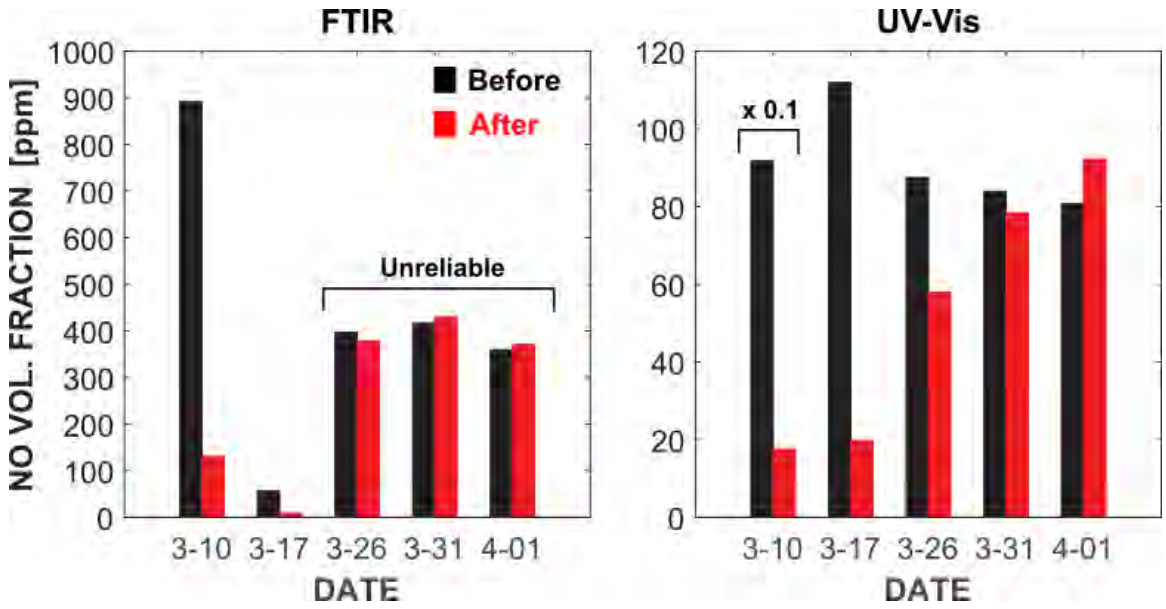

Figure 13. NO volume fraction before and after electron-beam treatment on different days

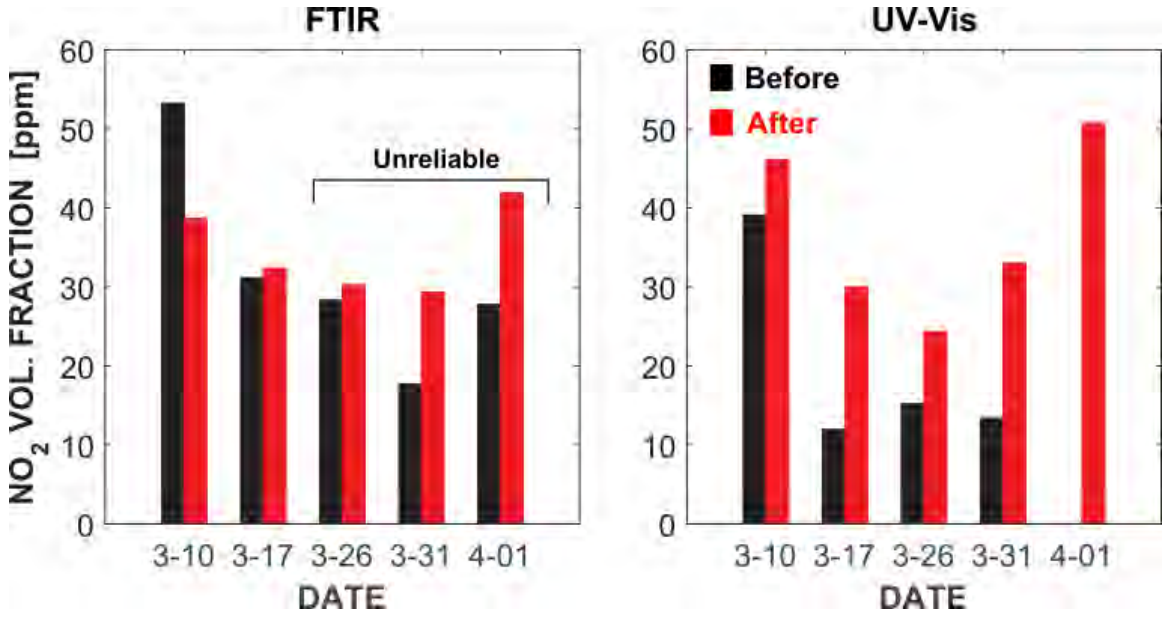

Figure 14. NO_2 volume fraction before and after electron-beam treatment on different days

As illustrated in the UV-Vis data (right column) of Figure 15, each level of added complexity for the initial gas mixture led to decreasing effectiveness of the e-beam in terms of NO_X reduction. For the simplest case of 1000 ppm NO_X in N_2 (03-10-2015), NO_X reduction was ~80% (i.e., final value was ~20% of initial value). When the gas mixture was changed to dry SFG (03-17-2015), NO_X reduction was ~55%. When the gas mixture was changed to humid SFG (03-26-2015), NO_X reduction was only ~20%. When the humid SFG was heated (03-31-2015), NO_X *increased* by ~15%. Finally, when the heated humid SFG was treated with higher e-beam energy (04-01-2015), NO_X *increased* by ~75%.

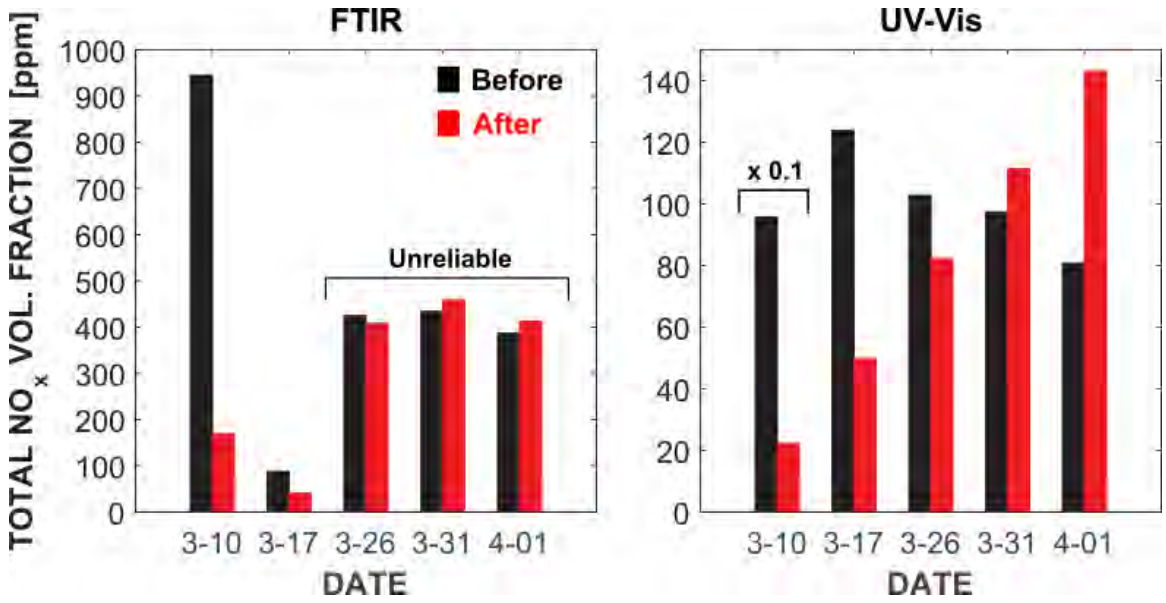

Figure 15. Total NOx volume fraction before and after electron-beam treatment on different days

It appears that the presence of water vapor is a "game changer," in that it by itself significantly reduces the effectiveness of the e-beam and can, combined with other factors such as heating, actually lead to *production* rather than reduction of NO_X. In addition, water vapor appears to interact with SO_2 in the SFG mixture, as evidenced by the lack of clear SO_2 absorption features in the relevant UV-Vis spectra (i.e., on 03-26, 03-31, and 04-01) both before and after e-beam treatment. Clearly, more work is needed to investigate the effect of water vapor (by itself or combined with other factors such as heating) on flue-gas chemistry and electron-beam effectiveness.

SUMMARY AND RECOMMENDATIONS

We have examined the use of a pulsed electron-beam system to reduce NO_X emissions in coal combustion flue gases. Single beam shots were applied to gases for various conditions on different days, and gas samples extracted before and after each beam shot were optically probed using both FTIR and UV-Vis spectrometer instruments. In these measurements, the following observations were made:

1. When water vapor was present, its absorption features interfered with the ability to perform FTIR measurements of NO, NO_2, and SO_2. Under these circumstances, however, it was possible to perform UV-Vis measurements of these species.
2. For these experiments, N_2O levels were too low to make meaningful FTIR measurements.
3. Effectiveness of the electron beam in reducing NO_X was significantly reduced by the presence of water vapor.

4. Effectiveness of the electron beam in reducing NO_X was further reduced when humidified gas was heated. This combination actually led to an increase in NO_X when the gas was treated with an e-beam pulse.
5. Effectiveness of the electron beam in reducing NO_X was even further reduced when heated humidified gas was treated with higher e-beam pulse energy. This combination led to an even higher increase in NO_X than when the beam energy was lower.

From the experimental data and some fundamental chemical-kinetic computations, the following conclusions have been reached:

1. FTIR measurements of NO, NO_2, and SO_2 would likely require dehumidification of the gas.
2. FTIR measurements of N_2O would likely require a gas cell with longer path length.
3. For the pulsed electron beam to be an effective tool for reducing NO_X, it would likely be necessary to either dehumidify the gas upstream or to introduce a chemical additive which could modify the detrimental effects of water on the NO_x decomposition mechanism.

Future Work

There appears to be great potential for the use of this pulsed electron-beam system for flue-gas treatment. Nevertheless, much work is still needed to prove this and to optimize the system. Future work may include:

- Detailed calibrations of FTIR and UV-Vis absorption signals, including concentration ranges closer to actual expected levels
- Replicate measurements to determine repeatability and to estimate statistical uncertainty
- Measurements using a gas cell with a longer path length, for greater sensitivity
- Measurements for dehumidified gas samples, to eliminate water vapor interferences
- Experimentation with possible chemical additives to mitigate the issues caused by presence of water vapor

ACKNOWLEDGEMENTS

The authors gratefully acknowledge the contributions of and discussions with the following individuals from NRL Code 6733: M. Myers, F. Hegeler and J. Sethian (retired). The authors also would like to acknowledge technical support from J. Dubinger of NRL Code 6733, A. Mangassarian of Leidos, and J. Picciotta of Berkeley Research Associates. The authors acknowledge helpful discussions with Andrew P. Baronavski of Envisioneering, Inc, and Steven Tuttle of NRL Code 6185. We are most grateful to John Russell, Code 6170, for his assistance in establishing this collaborative effort between the Chemistry Division and Plasma Physics. This work was supported by Zerronox Corporation (Zerronox) through a CRADA.

REFERENCES

[1**]** Cotton, F., Albert, Wilkinson, Geoffrey, *Advanced Inorganic Chemistry*, New York, Interscience Publishers (1972) 3rd edition.

[2] Holleman, A. F., Wiberg, E., *Inorganic Chemistry*, San Diego, Academic Press (2001) ISBN 0-12-352651-5.

[3] J.D. Sethian, M. Myers, I.D. Smith, V. Carboni, J. Kishi, D. Morton, J. Pearce, B. Bowen, L. Schitt, O. Barr, W. Webster, "Pulse Power for a Rep-Rate, Electron Beam Pumped KrF Laser," IEEE Trans. Plasma Sci. **28**, 1333 (2000).

[4] J.D. Sethian, M. Friedman, J.L. Giuliani Jr., R.H. Lehmberg, S.P. Obenschain, P. Kepple, M. Wolford, F. Hegeler, S.B. Swanekamp, D. Weidenheimer, D. Welch, D.V. Rose, and S. Searles, "Electron Beam Pumped KrF Lasers for Fusion Energy," Phys. Plasmas **10**, 2142 (2003).

[5] M.F. Wolford, M.C. Myers, J.L. Giuliani, J.D. Sethian, P.M. Burns, F. Hegeler, R. Jaynes, "Repetition-Rate Angularly Multiplexed Krypton Fluoride Laser System," Optical Engineering **47**, 104202 (2008).

[6] M.F. Wolford, M.C. Myers, F. Hegeler, J.D. Sethian, "NO_x Removal with Multiple Pulsed Electron Beam Free of Catalysts or Reagents," Phys. Chem. Chem. Phys. **15**, 4422 (2013).

[7] F. Hegeler, D.V. Rose, M.C. Myers, J.D. Sethian, J.L. Giuliani, M.F. Wolford, M. Friedman, Phys. Plasmas **11**, 5010 (2004).